Long-range resonance transfer of electronic excitations in close-packed CdSe quantum-dot solids

C. R. Kagan, C. B. Murray, and M. G. Bawendi
Massachusetts Institute of Technology, 77 Massachusetts Avenue, Cambridge, Massachusetts 02139
(Received 9 April 1996)

We show spectroscopically that electronic energy transfer in close-packed CdSe quantum-dot (QD) solids arises from dipole-dipole interdot interactions between proximal dots. We use cw and time-resolved photoluminescence to study electronic energy transfer in optically thin and clear, close-packed QD solids prepared from CdSe QD samples tunable from 17 to 150 Å in diameter ($\sigma<4.5\%$). High-resolution scanning electron microscopy and small-angle x-ray scattering are used to build a well-defined structural model for the QD solids. In mixed QD solids of small and large dots, we measure quenching of the luminescence (lifetime) of the small dots accompanied by enhancement of the luminescence (lifetime) of the large dots consistent with electronic energy transfer from the small to the large dots. In QD solids of single size dots, a redshifted and modified emission line shape is consistent with electronic energy transfer within the sample inhomogeneous distribution. We use Förster theory for long-range resonance transfer through dipole-dipole interdot interactions to explain electronic energy transfer in these close-packed QD solids. [S0163-1829(96)00932-0]

I. INTRODUCTION

Nanometer size semiconductor crystallites or quantum dots (QD's), small compared to the bulk exciton Bohr radius, exhibit size-dependent electronic and optical properties as electronic excitations are spatially confined to within the volume of the dot. Quantum confinement effects induce quantization of the bulk band structure, concentrating the bulk oscillator strength in discrete electronic transitions that shift to higher energy with decreasing dot diameter.[1] Synthesis of CdSe QD samples monodisperse to within atomic roughness[2] has made it possible to observe, assign, and monitor the size evolution of a series of excited electronic states.[3,4] These samples show strong band-edge emission with quantum yields (QY's) ranging from 0.1 to 0.9 at 10 K. The size-dependent optical absorption and emission spectra of ''single'' CdSe QD's have been deduced using transient differential absorption,[3] photoluminescence excitation,[4] and fluorescence line narrowing[5,6] spectroscopies. Agreement between experimental observations and theoretical calculations provides a framework for understanding the size-dependent electronic structure of individual CdSe QD's.[4–7]

Building close-packed solids from semiconductor QD's presents opportunities to investigate both the cooperative physical phenomena that develop as proximal QD's interact and the electronic and optical properties of QD solid-state materials. QD solids provide media for potential novel electronic, optical, and optoelectronic applications that combine the unique properties of individual QD's and the collective properties of coupled QD's. For example, dipole-dipole interdot interactions in close-packed QD solids are expected to further enhance the already increased optical nonlinearity of the individual QD (Ref. 8) as electronic excitations collect oscillator strength from multiple dots in the solid.[9] Dipolar coupling between proximal dots in close-packed solids also provides a structure of wireless interconnects mimicking the requirements for complex computations in cellular automata.[10,11] Coupled QD structures are the basis for designs of high optical gain, low threshold current QD lasers, and resonant tunneling QD devices.[12] Recently electroluminescence from densely packed layers of CdSe QD's combined with semiconducting polymers has been demonstrated.[13] Porous films prepared from nanocrystalline semiconductors have been used to transport charge in photoelectrochemical cells.[14] Optical and electronic characterization of QD solid-state materials is important in understanding the physics of interdot couplings and their role in determining the fate of electronic carriers and excitations generated in QD structures. Tailoring the size of and spacing between the QD's in solids presents opportunities to engineer on the nanometer scale the electronic, optical, and structural properties of these materials.

Recent advances in the fabrication of structurally well-defined two- and three-dimensional close-packed QD structures by photolithography,[10] molecular-beam epitaxy,[15] and wet chemical methods[16,17] makes the investigation of interdot couplings possible. Two-dimensional arrays of photolithographically patterned AlGaAs-GaAs QDs show additional absorption resonances in the infrared as neighboring dots become coupled.[10] Three-dimensional, close-packed CdSe and CdS QD solids have luminescence spectra shifted to the red of spectra for dispersed QD's, indicative of interdot interactions in the solid state.[16,17] In a recent paper we reported on optical studies of close-packed QD solids designed from a mixture of small and large CdSe QD's.[18] The small and large dots have well-separated spectral features, which allowed us to identify changes in their optical spectra. We measured quenching of the luminescence (lifetime) of the small dots accompanied by enhancement of the luminescence (lifetime) of the large dots. Photoluminescence excitation studies revealed that photoexcitations generated in both the small and large dots contribute to the luminescence of the large dots. We presented preliminary analysis showing that our observations are consistent with long-range resonance transfer of electronic excitations from the small to the large dots in the mixed QD solid. Here we present a more detailed analysis of our observations in the mixed QD solid to further demonstrate that dipolar coupling between proximal dots in

close-packed QD solids leads to electronic energy transfer. We show spectroscopically that in ''single'' size QD samples electronic energy transfer within the sample inhomogeneous distribution accounts for the red shift in the emission for the QD solid relative to that for the QD's dispersed in solution.

II. EXPERIMENT

Samples of CdSe QD's tunable in size from 17 to 150 Å in diameter with standard deviations less than 4.5% were synthesized according to Ref. 2. The preparation of these dots involves injecting Cd and Se sources into a hot coordinating solvent and growing nucleated CdSe seeds to the desired dot size. Postfabrication processing using size-selective precipitation further narrows the sample size distribution and isolates the dots from the organic growth medium leaving each CdSe core derivatized by an organic monolayer. These CdSe QD samples have been structurally and optically well characterized.[2–6,19] The organic capping groups sterically stabilize the dots in solution. Optically thin and transparent (nonscattering), close-packed QD solids were deposited from solutions of these QD samples.[17]

A JEOL JSM 6320FV high-resolution scanning electron microscope (HRSEM) was used to image QD's in close-packed solids prepared from pure samples of single size dots and from mixed samples of small and large dots. The microscope was operated at 30 kV to detect secondary electron emission from the CdSe QD solids deposited on silicon wafers. A conventional Rigaku 300 Rotoflex powder diffractometer equipped with a Cu anode was used to acquire small-angle x-ray scattering (SAXS) patterns for a size series of CdSe QD samples close packed into solids and dispersed at 1 wt. % in poly(vinyl butyral) (PVB). The diffractometer was operated in the Bragg configuration. Samples were deposited on machined (100) silicon wafers.

We optically study QD solids and solutions prepared from pure samples of single dots, mixed samples of small and large dots, and a broad sample distribution obtained by mixing five QD samples incremented by ~2 Å in dot diameter. The optical density (OD) of the thin QD solids was always less than 0.3 at the peak of the first excited state to minimize reabsorption of emitted photons. In the mixed solid, the OD of the large dots at the emission peak of the small dots was less than 0.05 so that absorption of the luminescence from the small dots by the large dots was negligible. The close-packed CdSe QD solids were deposited on sapphire flats for optical measurements at cryogenic temperatures. A Teflon spacer was used to separate the QD solids from a second sapphire window. Solutions of CdSe QD's were prepared by either dispersing the QD's in alkanes or in *n*-butyl benzene, a low-temperature glass former. Luminescence QY's for the QD solids and solutions were measured relative to the known luminescence intensities of organic dyes. Dispersions of CdSe QD's and solutions of organic dyes were loaded into sample holders between two sapphire flats separated by either a Viton O ring or Teflon spacer. Sample holders were mounted in a helium cryostat.

We used either a 300-W Hg-Xe arc lamp or a 100-W quartz-tungsten-halogen lamp to collect optical absorption spectra. The 457.9-nm line from an argon-ion laser or the Hg-Xe lamp in combination with a monochrometer was used as the excitation source in cw photoluminescence (PL) measurements. The transmitted or emitted light was dispersed through a 0.33-m monochrometer and the colors separated by either a 150-groove/mm or 300-groove/mm grating. The spectra were detected by an optical multichannel analyzer. Some cw PL spectra were collected using a SPEX Fluorolog-2 spectrofluorometer.

PL decays were measured using time-correlated single photon counting. The samples were excited by 2.143-eV (580-nm) and 2.302-eV (540-nm) picosecond pulses generated by a cavity dumped dye laser synchronously pumped with the third harmonic of a mode-locked Nd:YAG laser (where YAG denotes yttrium aluminum garnet). The setup was operated at a 1-MHz repetition rate with an overall time resolution of ~80 psec.

III. OBSERVATIONS AND ANALYSIS

A. Structural characterization

We use the HRSEM to image the QD's building up the three-dimensional QD solids. Figure 1(a) shows a QD solid prepared from 56-Å CdSe QD's. The inset shows the same sample imaged at higher magnification. The micrographs reveal that the QD's are close packed, forming a glassy solid in which each dot remains separated from its neighbors by the organic capping groups. In solids prepared from a mixture of small and large dots, the arrangement of the dots in the solids depends on the degree to which the dots order during deposition. We control the preparation of ordered and glassy QD solids by tailoring the solvents from which the QD samples are deposited.[17] Figure 1(b) shows a QD solid prepared from a mixture of 82% 37.5-Å and 18% 57-Å CdSe QD's. The small and large dots have phase separated into ordered regions. Figure 1(c) shows that in a glassy QD solid, prepared from 82% 38.5-Å and 18% 62-Å CdSe QD's, the small and large dots remain intermixed. We study electronic energy transfer from the small to the large dots in the well-intermixed glassy QD solids.

SAXS is used to characterize the average local structure of the QD's in the glassy solids. Figure 2(a) shows scattered intensities from a size series of CdSe QD samples dispersed in films of PVB (filled circles). Each of the QD's in a sample acts as an independent scattering center in the polymer matrix and adds to the total scattered intensity. The observed ringings are characteristic of the size and shape of the QD's in the samples. We account for background scattering from the PVB matrix by subtracting the scattered intensity from an undoped PVB film. The scattering pattern $I(s)$ for an individual, idealized spherical QD of radius R and of uniform electron density is represented by[20]

$$I(s)=f(s)^2=\left[(\rho-\rho_0)\,\frac{4}{3}\,\pi R^3\right]^2 \times\left[9\,\frac{[\sin(2\pi Rs)-2\pi as\,\cos(2\pi Rs)]^2}{(2\pi Rs)^6}\right], \tag{1}$$

where $f(s)$ is the Fourier transform of the form factor for a sphere and ρ and ρ_0 are the electron densities of the QD's and the polymer matrix. Equation (1) describes the oscillations observed in the SAXS patterns [Fig. 2(a)], accounting

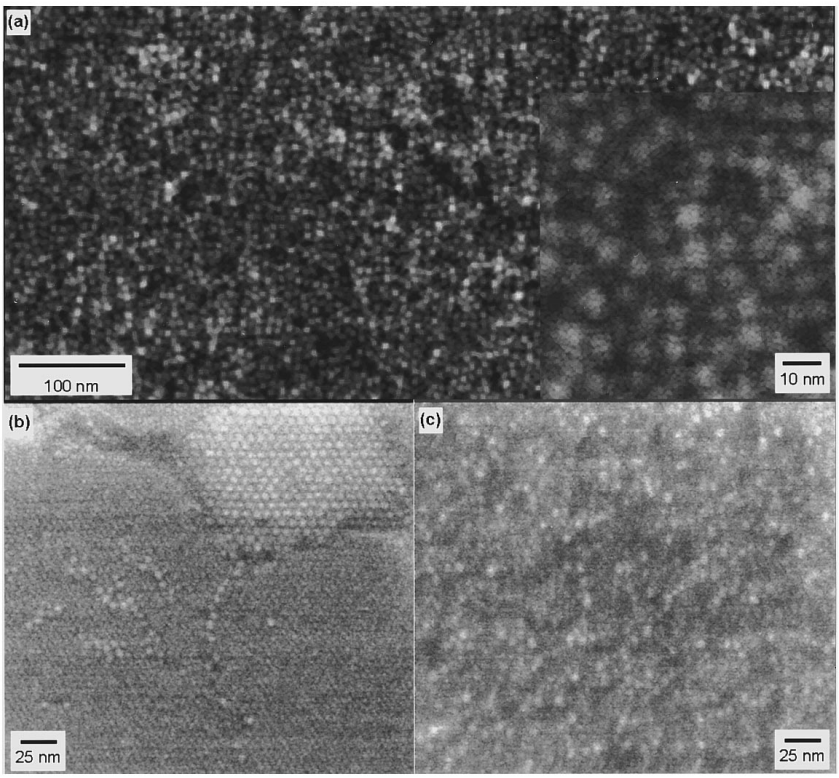

FIG. 1. (a) Lower and higher (inset) magnification HRSEM micrographs showing 56-Å CdSe QD's close packed in a glassy solid. Each dot remains separated from neighboring dots by the organic cap. (b) HRSEM micrograph of a mixed CdSe QD solid prepared from 82% 37.5-Å dots and 18% 57-Å dots. The mixture of dots is phase separated into ordered regions of the 37.5-Å dots and the 57-Å dots. (c) HRSEM image of a mixed CdSe QD solid prepared from 82% 38.5-Å and 18% 62-Å dots shows that the dots remain well intermixed when close packed in a glassy solid.

[1]for the decrease in periodicity with increasing dot diameter and the decrease in scattered intensity with increasing period. We resolve as many as five oscillations in the scattered intensities. These oscillations, long observed in classic colloidal systems,[20] were unresolved in previous studies of QD's where larger polydispersities broadened the oscillations and prevented their observation. Diffuse scattering of x rays off the differing electron densities of the Cd and Se atoms in the QD's adds to the base line in our SAXS patterns. The contribution from diffuse scattering proportional to R^3 is small compared to $f(s)^2 \propto R^6$ in micrometer size particles but becomes significant on the nanometer scale. TEM observations and the relative intensities of reflections in the wide-angle region of the diffraction patterns reveal that the QD's become prolate with increasing dot size with aspect ratios ranging from 1.0 to 1.25.[2] We simulate the SAXS patterns by simultaneously fitting the small- and wide-angle regions of the diffraction patterns to account for the internal structure of the QD and for its size-dependent aspect ratio.[17] We also allow for a Gaussian distribution in dot size for each of our QD samples to weight the total scattered intensity. We fit (solid lines) each of the four SAXS patterns (open circles) [Fig. 2(a)] to extract average dot diameters for spheres of equivalent volume and sample size distributions. We obtain dot diameters ranging from 31.6 to 62.1 Å with standard deviations between 3.5% and 4.5%.

Figure 2(b) compares the scattered intensities for the four samples of dots dispersed in PVB (filled circles) with those for dots densely packed in QD solids (solid lines). The differences in the scattered intensities arise from interferences between dots as their positions become correlated in the solids. This is observed mainly as a reduction in the scattered intensity appearing as an additional peak at small angles. The scattered intensity for a QD solid is described by the expression[20]

$$I(s) = N f(s)^2 \left[1 + \int 4\pi r^2 [\rho(r) - \rho_0] \frac{\sin(sr)}{sr} \, dr \right], \quad (2)$$

where the term in large square brackets represents the contributions from interferences, $\rho(r)$ describes the dot density as a function of radial distance from a reference dot in the sample, and N is the number of QD's in the solid. Using the experimental form factors $f(s)$ obtained from the scattered intensities of QD's dispersed in PVB [filled circles, Fig. 2(b)], we Fourier transform the contributions from interferences to generate pair distribution functions[21] (PDF's)

$$g(r) = \frac{\rho(r)}{\rho_0} = 1 + \frac{1}{2\pi^2 r \rho_0} \int_0^\infty s \left(\frac{I(s)}{N f(s)^2} - 1 \right) \sin(sr) \, ds \quad (3)$$

for the close-packed QD solids [Fig. 2(c)]. The peak in the PDF represents the center-to-center distance between neighboring dots in the solid. The higher-order oscillations are replicas of this same distance. The four QD solids are composed of close-packed CdSe dots with an interdot spacing of 11 ± 1 Å maintained by the organic capping groups. The monodispersity of our QD samples enables us to fabricate QD solids with well-defined close-packed structures for optical studies.

B. Optical spectroscopy

The sizes of the QD's in our samples are smaller than the bulk exciton Bohr radius in CdSe (56 Å).[7] Excitation of a QD generates an electron-hole pair that is confined to and delocalized over the volume of the dot. The spectroscopic and photophysical properties of the QD are analogous to those of a large molecule. 10-K optical absorption and emission spectra of optically thin and clear (nonscattering), close-

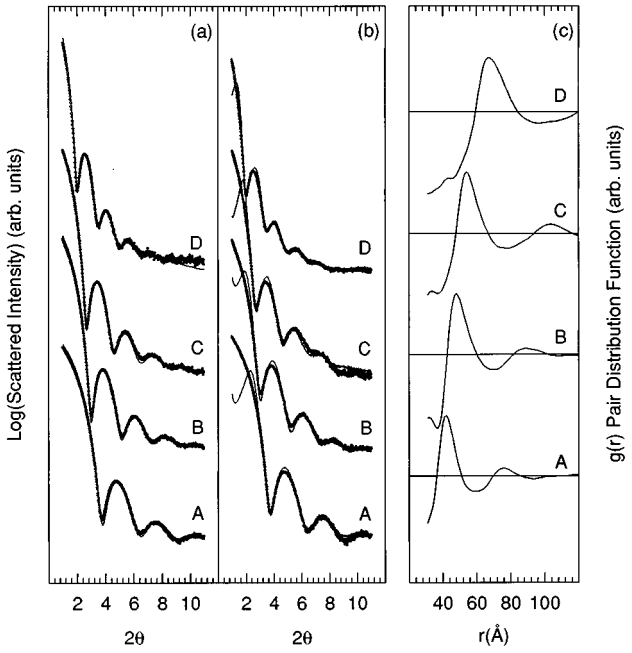

FIG. 2. (a) SAXS patterns for CdSe QD's dispersed (filled circles) in PVB and fit to form factors for dots (solid lines) (*A*) 31.6±4.0%, (*B*) 40.3±4.0%, (*C*) 45.6±4.0%, and (*D*) 61.0±4.2% in diameter. (b) Comparison of SAXS patterns for the four samples of CdSe QD's dispersed in PVB (filled circles) and close packed in QD solids (solid lines). (c) Pair distribution functions generated for the QD solids.

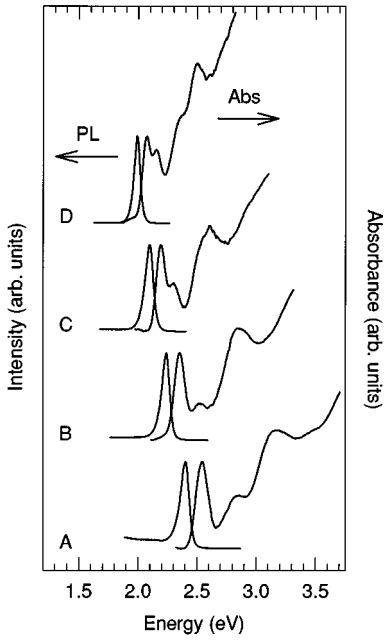

FIG. 3. 10-K optical absorption and emission spectra of optically thin and clear, close-packed QD solids prepared from samples of CdSe QD's (*A*) 30.3, (*B*) 39.4, (*C*) 48.0, and (*D*) 62.1 Å in diameter.

packed QD solids prepared from samples of CdSe QD's ranging in size from 30.3 to 62.1 Å in diameter are shown in Fig. 3. The discrete absorption resonances and sharp band-edge emission are characteristic of the size-dependent, quantized electronic excitations observed in these same CdSe QD samples dispersed in solution. The electronic and optical properties of the QD solid are similar to those of a molecular solid.

Electronic energy transfer between luminescent molecules in organic solids (chromophores) and between impurity centers in inorganic solids (phosphors) has been and remains an active area of research.[22] Electronic energy transfer encompasses any process by which electronic energy is transferred from an excited molecule or atom (the donor) to a ground-state molecule or atom (the acceptor), returning the donor to its ground state and promoting the acceptor to one of its higher excited states. Energy transfer is different from electronic transfer in that there is no net transport of charge; the charge neutral excitation is transferred as an entity from the donor to the acceptor. Radiationless transfer of electronic energy requires direct interaction between the excited donor and ground-state acceptor. It is a one-step process in which deexcitation of the donor and excitation of the acceptor occur simultaneously. It is distinct from radiative transfer in which an intermediate photon is first emitted from the donor and then reabsorbed by the acceptor with no direct donor-acceptor interaction.

At intermolecular-interatomic separations of 5–100 Å, in the range of the interdot separations in our solids, long-range resonance transfer (LRRT) is the dominant energy transfer mechanism.[22–24] LRRT of electronic excitations is a radiationless transfer process arising from coupling between the electromagnetic fields generated by the transition dipoles of resonant transitions in the excited donor and ground state acceptor. This donor-acceptor coupling is very weak so the rate of electronic energy transfer is slower than the rates of absorption and vibrational relaxation processes in the donor and acceptor. Electronic excitations are completely localized in the donor prior to being transferred to the acceptor. In systems of two dissimilar molecules, one the donor and the other the acceptor, LRRT is measured spectroscopically by the quenching of the luminescence QY or decrease in the luminescence lifetime of the donor or by the enhancement of the luminescence QY or increase in the luminescence lifetime of the acceptor. In order to observe LRRT, the acceptor must have both a transition resonant with the donor emission in which to accept the transferred excitation and a lower-energy state in which to trap the excitation.[22–24] Transfer of the excitation back to the donor is inhibited since no donor transition exists at that lower energy.

1. Mixed CdSe QD solid

We use the size dependence of the electronic spectrum of the QD's to create a mixed system of 82% 38.5-Å (small) dots and 18% 62-Å (large) dots in which to optically study electronic energy transfer in QD solids. In the mixed solid, the small dots are the donors and the large dots are the acceptors. Figure 4(a) is a cartoon representing the electronic transitions of the small and large dots. The large dot has a transition ($|g\rangle \rightarrow |A\rangle_1$) resonant with the emitting energy of the small dot ($|g\rangle \leftarrow |D\rangle$) and a lower energy state ($|A\rangle_2$) in which to trap the excitation. The excitation cannot be trans-

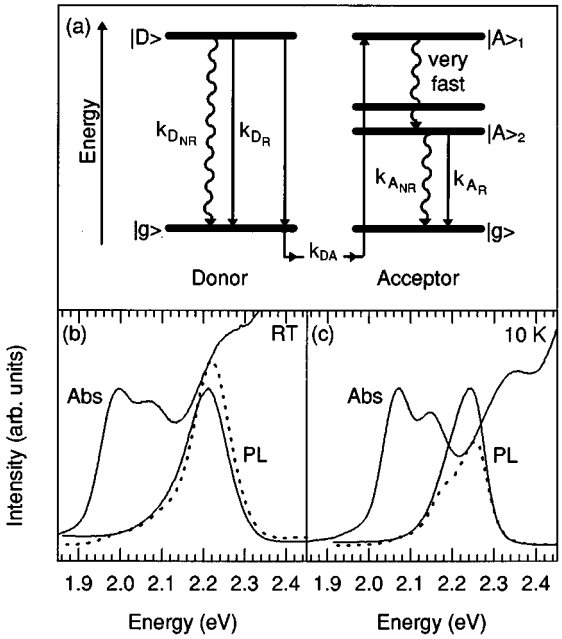

FIG. 4. (a) Cartoon depicting resonant transfer of electronic excitations from small (donor) to large (acceptor) CdSe QD's in a mixed QD solid. The energy levels shown are characteristic of the electronic spectra for the small 38.5-Å and large 62-Å QD's. $|g\rangle$ represents the ground states of the donor and acceptor, $|D\rangle$ is the lowest excited state of the donor, and $|A\rangle_1$ and $|A\rangle_2$ are a higher excited state and the lowest excited state of the acceptor, respectively. The large dot has both a transition resonant with the emission of the small dot and a lower energy state in which to trap transferred excitations. In addition to the radiative and nonradiative pathways for decay of photoexcitations, labeled by k_{D_R} and $k_{D_{NR}}$ for the small dots and by k_{A_R} and $k_{A_{NR}}$ for the large dots, electronic energy transfer labeled by the rate k_{DA} offers another pathway for deexcitation of the small dots and excitation of the large dots. (b) and (c) The RT and 10-K donor-acceptor resonance, respectively, are shown by spectral overlap (dotted lines) of the emission from the 38.5-Å dots with the absorption of the 62-Å dots.

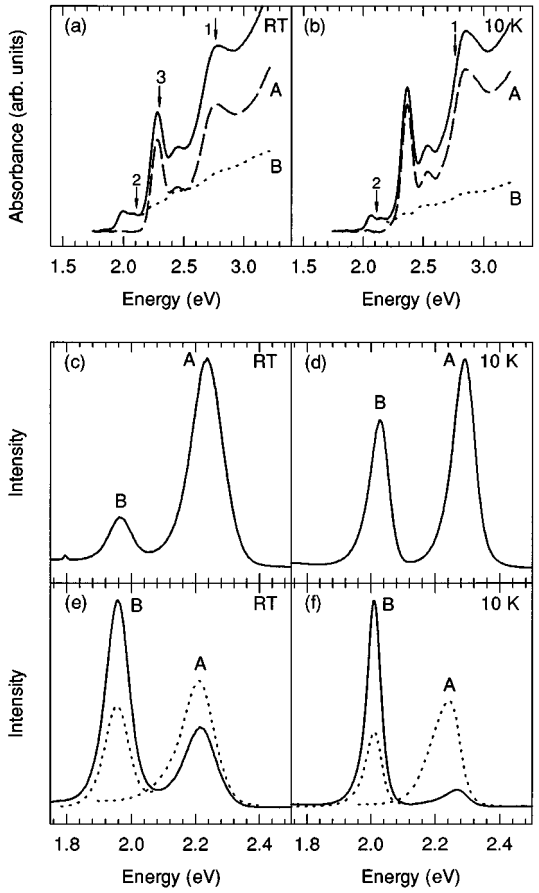

FIG. 5. Optical absorption spectra for a mixed CdSe QD solid prepared from 82% 38.5-Å dots and 18% 62-Å dots (solid lines) at (c) RT and (d) 10 K. The absorption spectra for the mixed QD solid are sums of the absorption spectra of its 38.5-Å (dashed lines) and 62-Å (dotted lines) QD components. Arrows indicate the (1) 2.762 eV (450 nm), (2) 2.143 (580 nm), and (3) 2.302 eV (540 nm) excitation energies used in cw and time-resolved PL measurements that are to the blue and red of the small dot absorptions. Emission spectra for the mixture of dots dispersed in solution at (c) RT and (d) 10 K and close packed in the QD solid at (e) RT and (f) 10 K. Dotted lines plot the relative QY's for 38.5-Å dots in a pure QD solid and for 62-Å dots exciting the mixed QD solid to the red of the small dot absorptions.

ferred back since the small dots are transparent at the lower energy. Figures 4(b) and 4(c) show the RT and 10-K donor-acceptor resonance (dotted lines) in the mixed QD solid calculated by overlapping the weighted emission spectrum of the small dots with the absorption spectrum of the large dots.

The absorption and emission features of the small and large dots in the mixed QD solid are spectrally well separated. RT and 10-K absorption spectra for the mixed QD solid are shown by solid lines in Figs. 5(a) and 5(b). Subtracting the spectral contributions from the large dots (dotted lines), we regain the spectra for the small dots (dashed lines) in the mixed QD solid. The absorption spectra for the mixed solid are sums of the absorption spectra of its small and large dot components. Electronic excitations are initially localized in individual small and large QD's in the solid.

A comparison of RT and 10-K luminescence spectra for the mixed system of dots dispersed in solution [Figs. 5(c) and 5(d)] with those for the dots close packed in the solid [solid lines, Figs. 5(e) and 5(f)] reveals a large increase in the ratio of the large to small dot luminescence QY's in the mixed solid. The samples were excited at 2.762 eV, labeled by arrow 1 in Figs. 5(a) and 5(b). Dotted lines in Figs. 5(c) and 5(d) plot the relative QY's for a pure, small QD solid (in the absence of large dots) and for the large dots in the mixed QD solid when excited to the red of the small dot absorptions. Excitation to the red of the small dot absorptions, labeled by arrow 2 in Figs. 5(a) and 5(b), excites only the large dots in the mixed QD solid. The QY's of the large dots are scaled by the relative QY's for large dots dispersed in solution when excited at the blue [arrow 1 in Figs. 5(a) and 5(b)] and red [arrow 2 in Figs. 5(a) and 5(b)] excitation energies. Scaling the QY's accounts for differences in source intensity and in the inherent QY's of the QD's at the two excitation energies. In luminescence, the spectra for the mixed QD

solid are no longer superpositions of the small and large dot luminescence spectra. Exciting both the small and large dots in the mixed QD solid [arrow 1 in Figs. 5(a) and 5(b)] reveals quenching of the luminescence QY of the small dots accompanied by enhancement of the luminescence QY of the large dots. Our observations are consistent with electronic energy transfer from the small to the large dots in the mixed QD solid. A comparison of RT and 10-K luminescence spectra shows that the magnitude of these effects increases at lower temperatures.

(a) Spectral overlap of donor emission and acceptor absorption. We calculate the probability (P_{DA}) and rate (k_{DA}) of electronic energy transfer from donor to acceptor in our QD solids in terms of spectroscopic quantities. Förster theory relates the efficiency of energy transfer due to donor-acceptor dipole-dipole interactions to the spectral overlap of donor emission and acceptor absorption.[22–24] Using the spectral overlap, shown by dotted lines in Figs. 4(b) and 4(c), we calculate the critical radius (R_0) for LRRT in our QD solids. R_0 is the distance between donor and acceptor at which k_{DA} equals the rate of donor deexcitation by competing mechanisms. R_0 is a measure of energy transfer efficiency relative to R_{DA}, the physical distance between donor and acceptor in the QD solid. For a random orientation of transition dipoles,[22–24]

$$R_0 \propto \left(\frac{\varphi_D}{n^4} \int_0^\infty F_D(\tilde{\nu}) \varepsilon_A(\tilde{\nu}) \frac{d\tilde{\nu}}{\tilde{\nu}^4} \right)^{1/6}, \tag{4}$$

where φ_D is the luminescence QY of the donor (0.0185 at RT and 0.2395 at 10 K), n is the refractive index of the QD solid, $F_D(\tilde{\nu})$ is the normalized spectrum for donor emission, and $\varepsilon_A(\tilde{\nu})$ is the molar extinction coefficient for acceptor absorption. We assume the transition dipoles are randomly oriented as the transition dipole is defined by the CdSe unit cell and each dot is randomly oriented in the glassy solid. We calculate n as the volume weighted average of that for the QD's [2.58 at RT and 2.54 at 10 K (Refs. 25 and 26)] and the organic cap (1.47 for trioctylphosphine[27]), assuming a randomly close-packed QD solid with the organic cap filling the interstices. The molar extinction coefficient for the small dots is calculated from its absorption spectrum using Beer's law, assuming that the molar extinction coefficient at the peak of the first excited state is $1\times10^6\ M^{-1}\ \mathrm{cm}^{-1}$. Using Eq. (4), we obtain R_0=47 Å at RT and 67 Å at 10 K. The temperature dependence of R_0 originates from the increased QY of the small dots with decreasing temperature.

(b) Time dependence of electronic energy transfer. The time dependence of the luminescence decays for the small and large dots in the mixed QD solid gives us an independent measure of R_0 and confirms the LRRT mechanism. Figure 4(a) shows that in addition to the radiative (R) and nonradiative (NR) decays in the small and large dots, electronic energy transfer with rate k_{DA} offers another pathway for deexcitation of the small dots and excitation of the large dots. Figure 6 (dotted lines) shows RT luminescence decays monitoring the peaks in the PL spectra of Fig. 5(e) for the small dots in the pure QD solid (a) and the mixed QD solid (b) and for the large dots exciting the mixed solid to the blue [arrow 3 in Fig. 5(a)] (c) and red [arrow 2 in Fig. 5(a)] (d) of the small dot absorptions. The peaks in the luminescence decays are normalized to compare their time dependence. Electronic energy transfer from the small to the large dots is observed as the decrease in the luminescence lifetime of the small dots and the accompanied increase in the luminescence lifetime of the large dots.

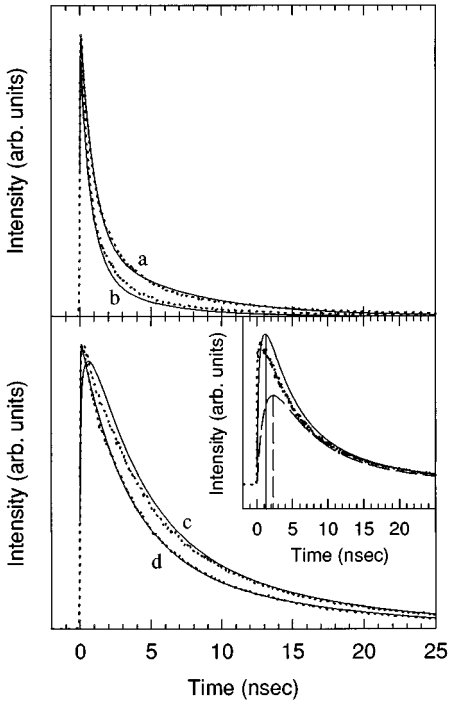

FIG. 6. Luminescence decays monitoring the emission peak of the 38.5-Å dots in a pure QD solid (a) and in the mixed QD solid (b) and for the 62-Å dots exciting the mixed QD solid to the blue (c) and red (d) of the small dot absorptions. The peaks in the decays are normalized to compare their time dependence. Decays for the (a) 38.5-Å and (d) 62-Å QD's in the absence of energy transfer are fit to biexponentials (solid lines). The decrease in the luminescence lifetime of the 38.5-Å dots in the mixed QD solid is fit by Förster's decay law for LRRT of electronic excitations [solid line (b)]. The increase in the luminescence lifetime for the large dots upon transfer of electronic excitations from the small dots is calculated for LRRT [solid line (c)]. The fit and calculated curves are scaled by their relative QY's to the experimental decays. The inset compares the energy transfer contribution to the decay of the large dots found experimentally (dotted lines) with the LRRT (solid line) and exciton diffusion (dashed line) mechanisms. The instrumental response was convoluted in all our fits and calculations.

The luminescence decays for the small dots in a pure QD solid (a) and for the large dots in the mixed QD solid excited to the red of the small dot absorptions (d) correspond to exciton decay times by radiative and nonradiative processes in the absence of energy transfer. We use nonlinear least-squares methods to fit these nonexponential luminescence decays by biexponentials (solid lines a and d), representing distributions of lifetimes for the QD's in the samples.[28] The excited-state populations for the small dots [$n_D(t)$] and the large dots [$n_A(t)$] including electronic energy transfer from the small to large dots are described by the rate equations[29]

$$\dot{n}_{D_i}(t) = G_{D_i}(t) - \frac{n_{D_i}(t)}{\tau_{D_i}} - k_{DA}(t) n_{D_i}(t)$$

$$\text{where} \quad n_D(t) = \sum_{i=1,2} n_{D_i}(t), \quad (5)$$

$$\dot{n}_{A_j}(t) = G_{A_j}(t) - \frac{n_{A_j}(t)}{\tau_{A_j}} + k_{DA}(t) n_D(t)$$

$$\text{where} \quad n_A(t) = \sum_{j=1,2} n_{A_j}(t), \quad (6)$$

where $G_{D_i}(t)$ [$G_{A_j}(t)$] represents the donors [acceptors] excited directly by the pulsed source, $n_{D_i}(t)$ [$n_{A_j}(t)$] is the time-dependent number of excited donors [acceptors] in the mixed QD solid with lifetime $\tau_{D_i}(t)$ [$\tau_{A_j}(t)$], and D_i (A_j) indexes the donors (acceptors) characterized by short and long lifetimes. We assume that all small dots have the same energy transfer rate k_{DA}. The time dependence of the luminescence distinguishes the two most common radiationless energy transfer mechanisms in solids, LRRT and exciton diffusion. LRRT has $k_{DA}(t) \propto t^{-1/2}$, while exciton diffusion has a time independent k_{DA}.[26]

(i) Long-range resonance transfer. Solving Eq. (5) for LRRT, we fit the decrease in the PL lifetime for the small dots in the mixed solid by Förster's decay law[29] (solid line *b*)

$$n_{D,\text{mixed}}(t) = n_{D,\text{pure}}(t) \exp\left[-\gamma \left(\frac{\pi t}{\overline{\tau_D}} \right)^{1/2} \right], \quad (7)$$

where $n_{D,\text{pure}}(t)$ is the biexponential fit (solid line *a*), $\overline{\tau_D}$ is the weighted average lifetime for the small dots in the pure QD solid, and $\gamma = C(\frac{4}{3}\pi R_0^3)$. C is the concentration of large dots in the mixed QD solid and is calculated using Beer's law and the film thickness measured by profilometry. R_0 is then the only adjustable parameter in the fit that yields $R_0 = 48$ Å.

Using Eq. (7) to solve Eq. (6), we calculate the increase in the luminescence lifetime for the large dots in the mixed solid as[29]

$$n_{A,\text{blue}}(t) = n_{A,\text{red}}(t) + A_D \sum_{j=1,2} n_{A_j}(0) \int_0^t \exp\left(\frac{s-t}{\tau_{A_j}} \right) n_D(s) k_{DA}(s) ds. \quad (8)$$

The first term $n_{A,\text{red}}(t)$ is the biexponential fit (solid line *d*) to the luminescence decay for the large dots in the mixed QD solid when excited to the red of the small dot absorptions. It represents the contribution to the luminescence decay from photoexcitations generated directly in the large dots by the source. The second term describes the decay of large dot excitations that were resonantly transferred from the small dots. The integrand is proportional to the time-dependent LRRT rate and the exponent describes the decay of large dot excitations, with rate $(1/\tau_{A_i})$, generated at time s upon transfer from the small dots. We sum the contributions from dots characterized by lifetimes τ_{A_j} with weights $n_{A_j}(0)$. A_D represents the relative absorbance of the small to large dots at the blue excitation. The calculated curve for LRRT is shown by the solid line *c*. The calculated curve for LRRT reproduces both the time dependence of the experimental decay and the enhancement in the luminescence intensity for the large dots.

(ii) Exciton diffusion. Solving Eqs. (5) and (6) for exciton diffusion, we fit the decrease in the luminescence decay for the small dots and calculate a curve for the increase in the luminescence decay for the large dots. The fit to the decay for the small dots is similar to that found for LRRT and is not shown for clarity. We compare the experimental and modeled energy transfer decays in the inset of Fig. 6. The experimental data (dotted lines) are calculated by subtracting experimental curves *c* and *d* when scaled by their relative QY's. A comparison of the calculated curve for LRRT, shown by the solid line, and that for exciton diffusion, shown by the dashed line, shows that for the same average k_{DA}, LRRT leads to a more rapid transfer of energy than does exciton diffusion. The LRRT mechanism reproduces both the time dependence of the decay and the increase in the luminescence intensity for excitations transferred to the large dots, while exciton diffusion does not. This may be expected since exciton diffusion is the dominant energy transfer process for donor-acceptor separations of 2–5 Å.[23] The distance of closest approach in our QD solids is ~11 Å, the separation between the surfaces of neighboring dots.

(c) Quenching of the luminescence QY of the small QD's. We also calculate R_0 for LRRT in our QD solids by the quenching of the luminescence QY for the small dots in the mixed QD solid relative to that for the small dots in a pure QD solid. Integrating $n_{D,\text{pure}}(t)$ and Eq. (7), assuming a single weighted average lifetime for the small QD's, yields expressions for the luminescence QY's for the small dots in the pure and mixed solids. The ratio of their luminescence QY's (Ref. 29)

$$\frac{\varphi_{D,\text{mixed}}}{\varphi_{D,\text{pure}}} = 1 - \frac{\pi}{2} \gamma \exp\left(\frac{\pi \gamma^2}{4} \right) \text{erfc}\left(\frac{\pi^{1/2} \gamma}{2} \right) \quad (9)$$

is used to find γ, which yields values for $R_0 = 47$ Å at RT and 81 Å at 10 K.

(d) Summary. The spectral overlap of donor emission and acceptor absorption and the quenching of the luminescence QY of the donor give us independent measures of $R_0 = 47$ Å at RT and 67 and 81 Å, respectively, at 10 K. Time-dependent measurements at RT show that the LRRT mechanism for electronic energy transfer reproduces the luminescence decays for the small and large dots in the mixed QD solid with $R_0 = 48$ Å. A comparison of R_0 with the distance between donor and acceptor centers ($R_{DA} = 61.25$ Å), measured from SAXS data, reveals that dipolar coupling between QD's is a nearest-neighbor interaction. Using the average lifetime of the small dots from the luminescence decays (curve *a*, Fig. 6) and R_{DA} from SAXS data, we calculate k_{DA} for LRRT in our QD solids using $k_{DA} = (1/\tau_D)(R_0/R_{DA})^6$. We obtain $k_{DA} = 1 \times 10^8$ sec^{-1} at RT, consistent with characteristic rates for LRRT.[23] The relative rates of k_{DA} and $1/\overline{\tau_D}$ or the relative distances of R_0 and R_{DA} are used to calculate the probability of energy transfer P_{DA}, given by[30]

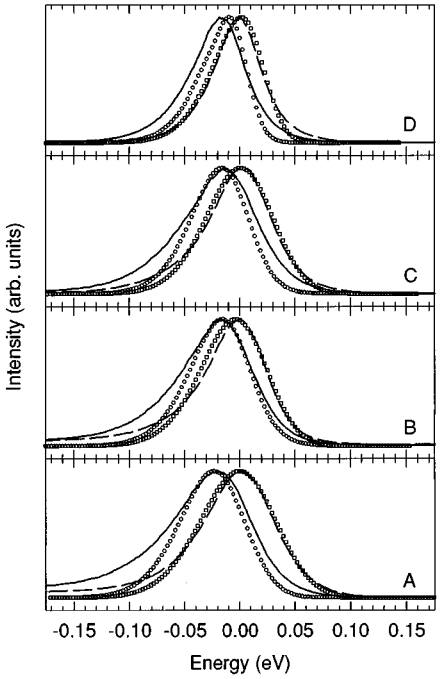

FIG. 7. Comparison of 10-K luminescence spectra for (*A*) 30.3-, (*B*) 39.4-, (*C*) 48.0-, and (*D*) 62.1-Å dots dispersed in solution (dashed lines) and close packed in QD solids (solid lines). Absorption spectra for these samples are shown in Fig. 3. The luminescence spectra are plotted relative to the luminescence peaks for the solutions. Fits to the solution spectra (open squares) are obtained by convoluting Gaussian inhomogeneous distributions with size-dependent ''single dot'' luminescence spectra. Simulated emission spectra (open circles) for the QD solids allow for energy transfer within the sample inhomogeneous distributions.

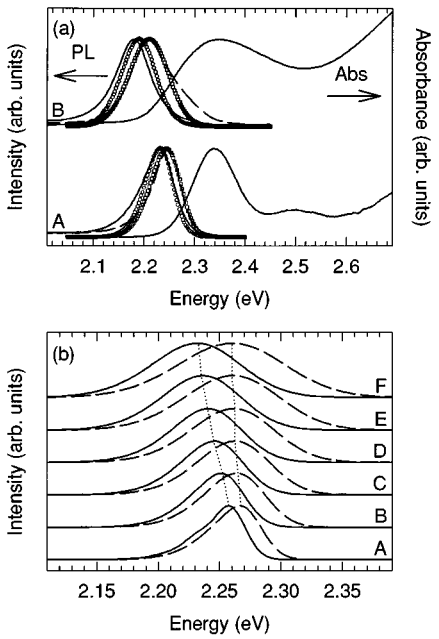

FIG. 8. (a) 10-K absorption and luminescence spectra for samples with (*A*) narrow and (*B*) broad sample inhomogeneous distributions dispersed in solution (dashed lines) and close packed in QD solids (solid lines). Simulated luminescence spectra (open squares) fit to the solution spectra and calculated spectra (open circles) allowing for energy transfer within each of the sample inhomogeneous distributions. (b) Calculated emission spectra for 39-Å CdSe QD samples with (*A*) 1.5%, (*B*) 2%, (*C*) 2.5%, (*D*) 3%, (*E*) 3.5%, and (*F*) 4% sample inhomogeneous distributions (dashed lines). Simulated emission spectra allowing for energy transfer within the sample inhomogeneous distributions (solid lines).

$$P_{DA}=\frac{k_{DA}}{k_{DA}+\dfrac{1}{\tau_D}}=\frac{R_0^6}{R_0^6+R_{DA}^6}. \tag{10}$$

Equation (10) yields energy transfer probabilities of 0.17 at RT and 0.63 at 10 K. The increase in P_{DA} also arises from the increase in QY for the small dots at 10 K and explains the increased magnitude of the energy transfer effects seen at low temperature in Figs. 5(e) and 5(f).

2. Single size CdSe QD solids

The absorption spectra of the QD solids and their parent solutions are indistinguishable. This suggests that electronic excitations are initially localized in the individual QD's. Figure 7 plots the 10-K luminescence spectra for the CdSe QD solids (solid lines) shown in Fig. 3 relative to those for the dots dispersed in a frozen solution (dashed lines). The emission line shapes for the QD solids are redshifted and accentuated on the red side of the distributions. The magnitude of the redshifts range from 15 to 35 meV at 10 K, varying from sample to sample, showing no discernible size dependence and decreasing with increasing temperature. The shifts are reversible upon redispersion of the QD solids. The absorption and luminescence spectra for the QD samples dispersed in matrices varying in polarity and in dielectric constant show no solvent effects.

(a) Sample inhomogeneous distribution. In each of our QD samples there still remains an inhomogeneous distribution in the emitting energies of our QD's. The full luminescence spectra for the samples dispersed in solution are each the sum of structured, ''single'' dot emission spectra. The structured fluorescence of the individual QD is washed out by sample spectral inhomogeneity. The origin of the inhomogeneous distribution is primarily from the size distribution. We use smaller and larger to refer to dots whose spectra are shifted to the blue and red relative to each other. Studies using fluorescence line narrowing spectroscopy optically select a subset of the sample inhomogeneous distribution, revealing the structured fluorescence characteristic of the individual QD.[5,6] The single dot emission spectrum is composed of a narrow band-edge emission and its LO-phonon progression, which we model by

$$E(\nu,\nu')=\sum_{n=0}^{4}\frac{1}{\sqrt{2\pi}\gamma_n}\frac{(S_e)^n}{n!}\exp\left(-\frac{[\nu-(\nu'-n\omega_{\mathrm{LO}})]^2}{2\gamma_n^2}\right), \tag{11}$$

where ν' is the position of the zero LO-phonon line in emission and S_e is the strength of the exciton–LO-phonon coupling in emission.[5,6] The sum is taken over the first five LO-phonon replicas, which are separated by the LO-phonon frequency for CdSe, ω_{LO}, and have linewidths γ_n. The parameters S_e and γ_n are a function of the size of the dot and are found in Ref. 5. Using the parameters for the average size QD in the sample, we fit the full luminescence spectra using nonlinear least-squares methods (open squares, Fig. 7) with the convolution integral[5,6]

$$E_{\mathrm{PL}}(\nu)=C\int E(\nu,\nu')D(\nu',\nu_0)d\nu'. \tag{12}$$

We assume that the sample inhomogeneous distribution $D(\nu',\nu_0)$ is a Gaussian function centered at ν_0 with standard deviation γ. C is a constant with the appropriate units.

(b) Probability of electronic energy transfer. Our observations (Fig. 7) are consistent with electronic energy transfer from the smaller to the larger dots within the sample inhomogeneous distribution.[31] Electronic energy transfer leads to quenching of the blue luminescence accompanied by enhancement of the red luminescence. This manifests itself as a redshift in peak position and an asymmetric and narrowed emission line shape. This is similar to what has been observed in the photosynthetic bacterium Rhodospirillium rubrum, where electronic energy transfer within a spectrally inhomogeneous distribution leads to a redshift in emission and an asymmetric line shape.[32]

We calculate an average R_0 for LRRT in each of our QD solids from spectral overlap, using Eq. (4). Now, $F_D(\tilde{\nu})$ is the normalized emission spectrum for the QD sample, given by the emission spectrum for the QD's dispersed in solution; $\varepsilon_A(\tilde{\nu})$ is the molar extinction coefficient for the QD's, obtained from the absorption spectrum of the QD solid; and φ_D is the luminescence QY of the QD solid. Luminescence QY's for the solids measured at 10 K (RT) range from ~0.01 to 0.2 (from ~0.001 to 0.01), a factor of ~10 lower than QY's measured for the dots in solution. A reduction in the QY's of the solids may arise in part from charge separation and transport between the dots, decreasing the probability of both the electron and hole residing in the same dot. Energy transfer to nonluminescing dots probably also contributes to quenching of the QY. We obtain values of R_0=37.9, 35.4, 47.3, and 53.9 Å for samples *A*, *B*, *C*, and *D*, respectively. The values for R_0 show an increase with the increased spectral overlap in samples of larger size QD's, but vary more significantly with the QY for the QD solid. This is seen for sample *B*, whose QY is lower than for the other three samples. A comparison of R_0 with R_{DA}=41.3, 50.4, 59.1, and 73.1 Å for samples *A*, *B*, *C*, and *D*, obtained from SAXS data, shows energy transfer in QD solids prepared from single size dots also arises from only nearest-neighbor interdot interactions. Using Eq. (10), we calculate P_{DA}=0.38, 0.11, 0.21, and 0.14 for each of the solids, *A*, *B*, *C*, and *D*. In general, values for P_{DA} show a decrease with increasing dot size as R_{DA} increases faster than R_0. Again P_{DA} varies with the QY of the solid, seen by the lower probability for sample B.

(c) Simulation of energy transfer within the sample inhomogeneous distribution. Starting with the luminescence profile for the inhomogeneous distribution of QD's dispersed in solution, we simulate energy transfer between each dot and its shell of nearest neighbors in a three-dimensional close-packed QD solid. The number of acceptors in the nearest-neighbor shell for a potential donor with excitation energy ν_{em_i},

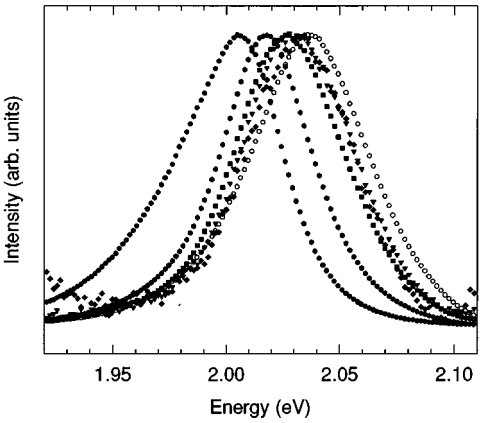

FIG. 9. 10-K luminescence spectra for 62-Å CdSe QD's close packed in a solid (filled circles) and dispersed in solution (open circles). Luminescence spectra for 62-Å QD's dispersed in matrices of 38.5-Å QD's shift blue with decreasing concentrations of the 62-Å QD's [18% (filled hexagons), 6.2% (filled squares), 3.2% (filled triangles pointed down), and 2.1% (filled diamonds)] approaching the luminescence of the dots dispersed in solution.

$$N_A(\nu_{\mathrm{em}_i})=\frac{12}{\sqrt{2\pi}\gamma}\int_{-\infty}^{\nu_{\mathrm{em}_i}}\exp\left[-\frac{(\nu-\nu_0)^2}{2\gamma^2}\right]d\nu, \tag{13}$$

is represented by the probability that the 12 proximal dots are larger in size, having lower-energy states ($\nu\leqslant\nu_{\mathrm{em}_i}$). Again, transfer of energy from larger to smaller dots is not possible since the smaller dots are transparent to the lower-energy excitations in the larger dots.

The probability that dots within the sample inhomogeneous distribution are not quenched by energy transfer to larger dots and emit their energy is given by

$$D(\nu_{\mathrm{em}_f}=\nu_{\mathrm{em}_i})=\frac{1}{\sqrt{2\pi}\gamma}\exp\left[-\frac{(\nu_{\mathrm{em}_i}-\nu_0)^2}{2\gamma^2}\right]\times(1-P_{DA})^{N_A(\nu_{\mathrm{em}_i})}, \tag{14}$$

where ($\nu_{\mathrm{em}_f}=\nu_{\mathrm{em}_i}$) indicates that the energy of the photons emitted is equivalent to the initial energy in the dots. As the concentration of neighboring acceptors increases for the smaller dots in the distribution, the probability that they are quenched by larger dots increases. The probability that dots with energy ν_{em_i} are quenched and their energy transferred to and emitted from acceptors at $\nu_{\mathrm{em}_f}\leqslant\nu_{\mathrm{em}_i}$ is described by the integral

$$A(\nu_{\mathrm{em}_f}) = \int_{\nu_{\mathrm{em}_f}}^{\infty} \frac{\frac{12}{2\pi\gamma^2}\exp\left[-\frac{(\nu_{\mathrm{em}_f}-\nu_0)^2}{2\gamma^2}\right]\exp\left[-\frac{(\nu_{\mathrm{em}_i}-\nu_0)^2}{2\gamma^2}\right]\left[1-(1-P_{DA})^{N_A(\nu_{\mathrm{em}_i})}\right]}{N_A(\nu_{\mathrm{em}_i})}\, d\nu_{\mathrm{em}_i}. \quad (15)$$

We assume that transfer to and emission from any of the acceptors is equally probable. The emission spectrum for the QD solid is then a sum of the emission from dots that were not quenched, $D(\nu_{\mathrm{em}_f}=\nu_{\mathrm{em}_i})$, plus the emission from acceptors that were enhanced, $A(\nu_{\mathrm{em}_f})$, upon energy transfer from a donor with energy $\nu_{\mathrm{em}_i} \geqslant \nu_{\mathrm{em}_f}$. The luminescence spectra calculated for each of the QD solids are shown by open circles in Fig. 7. The simulated spectra that allow for energy transfer within the sample inhomogeneous distributions reproduce the experimentally observed red shift. The quality of the simulated spectra relies on our ability to initially fit the sample inhomogeneous distribution. The inability of a Gaussian distribution to reproduce the red tail in the luminescence of dots dispersed in solution becomes magnified in the solids as energy transfer from the small to the large dots enhances the red tail of the luminescence.

(d) *Effects of the sample inhomogeneous distribution.* Figure 8(a) compares the 10-K absorption and luminescence spectra for QD solids and dispersions prepared from samples averaging 39 Å in diameter with a narrow ~4.5% (sample *A*) and a broad ~12% (sample *B*) inhomogeneous distribution. The states resolved in the absorption spectrum of sample *A* are obscured in *B* by the increased polydispersity. The linewidth in luminescence is also broadened by the increased inhomogeneous distribution of *B*. A comparison of the luminescence spectra for the narrow and broad samples dispersed in solutions (dashed lines) and close packed in solids (solid lines) reveals an increase in the magnitude of the redshift for the solid with increased inhomogeneous distribution. The magnitude of the redshift for sample *A* is 14.6 meV, while that for sample *B* is 29.6 meV. Close inspection reveals a small narrowing of the emission line shape for the QD solid for sample *A* [difference between solution and solid of 11.2 meV full width at half maximum (FWHM)] and a noticeable, larger narrowing of the emission line shape for the QD solid for sample *B* (difference between solution and solid of 22.9 meV FWHM). The increased magnitude of the redshift and the narrowing of the emission line shape with increasing inhomogeneous distribution are observed at both RT and 10 K.

We again fit the luminescence of the solutions (open squares) and simulate the expected luminescence of the solid, assuming energy transfer within the distribution (open circles). The simulated spectra show that energy transfer within the sample inhomogeneous distribution accounts for both the increased redshift and narrowing of the emission line shape with the larger distribution of sample *B*.

Figure 8(b) illustrates the expected dependence of the redshift on size distribution. Figure 8(b) shows simulated emission spectra for six 39-Å dot samples with increasing inhomogeneous distributions if dispersed in solution (dashed lines) and close packed in QD solids (solid lines). P_{DA} for LRRT in each of the six simulated QD solids is kept constant at 0.25. The dotted lines are used to follow the peaks of spectra. Increasing the sample inhomogeneous distribution for the QD's dispersed in solution broadens and slightly redshifts the simulated emission line shape. The spectra for the solids show that the magnitude of the redshift and the narrowing of the emission line shape becomes more prominent with increased spectral inhomogeneity. The magnitude of the redshift in the luminescence of the solids is not a simple measure of energy transfer efficiency. The redshift reflects both the efficiency of energy transfer and the spectral inhomogeneity of the QD sample.

(e) Concentration dependence of electronic energy transfer. Figure 9 shows the PL spectra for 62-Å CdSe QD's dispersed in solution (open circles) and closely packed in QD solids (filled circles). To further understand the observed redshift and modified emission line shape for the QD solids, we dispersed varying concentrations of the 62-Å QD's in matrices of smaller 38.5-Å QD's, producing glassy solids. Decreasing the concentration of the 62-Å dots increases their average separation and the probability that two large dots will be nearest neighbors. As the concentration of the 62-Å dots is decreased, the PL spectra of the 62-Å dots shifts blue approaching the solution luminescence at the lowest concentration. The emission lineshape for the dots also regains its ''Gaussian'' appearance as the dots are diluted in the matrix of smaller dots.

IV. CONCLUSION

The physics of interdot interactions between proximal QD's is important in understanding the fate of electronic carriers and excitations generated in QD structures. In this paper, we present spectroscopic evidence of electronic energy transfer in close-packed CdSe QD solids arising from dipole-dipole interdot interactions between proximal dots. In a mixed system designed from small and large dots, electronic energy transfer from the small to the large dots is observed as luminescence quenching of the small dots and luminescence enhancement of the large dots. Using Förster's theory for LRRT, we obtain independent and consistent measures of the energy transfer efficiency from spectral overlap considerations and from the quenching of the luminescence of the small dots in the mixed QD solid. The decrease in the luminescence decay for the small dots and the increase in the luminescence decay for the large dots is reproduced by the LRRT model with the same energy transfer efficiency. In QD samples of single size dots, electronic energy transfer within the sample inhomogeneous distribution reproduces the observed red shift and narrowing of the emission line shape in close-packed QD solids. These effects of energy transfer on the emission line shape for the QD solid become more prominent as the inhomogeneous distribution of the sample increases. A comparison of R_0 with the distance be-

tween neighboring QD's reveals that electronic energy transfer in QD solids arises from nearest-neighbor dipole-dipole interactions.

ACKNOWLEDGMENTS

The authors would like to thank Manoj Nirmal for assistance collecting luminescence decays. C. R. K. benefited from a NSF Training Grant in Environment Chemistry (Grant No. CHE92-56458). M. G. B. thanks the David and Lucille Packard Foundation and the Sloan Foundation for financial support. This research was funded in part by NSF (Grant No. DMR-91-57491) and by the NSF-MRSEC program (Grant No. DMR-94-00034). We also thank the MIT Harrison Spectroscopy Laboratory (Grant No. NSF-CHE-93-04251) for support and use of its facilities.

[1] Al. L. Efros and A. L. Efros, Fiz. Tekh. Poluprovodn. 16, 1209 (1982) [Sov. Phys. Semicond. **16**, 772 (1982)]; L. E. Brus, J. Chem. Phys. **80**, 4402 (1984).

[2] C. B. Murray, D. J. Norris, and M. G. Bawendi, J. Am. Chem. Soc. **115**, 8706 (1993).

[3] D. J. Norris and M. G. Bawendi, J. Chem. Phys. **103**, 5260 (1995).

[4] D. J. Norris and M. G. Bawendi, Phys. Rev. B **53**, 16 338 (1996).

[5] D. J. Norris, Al. L. Efros, M. Rosen, and M. G. Bawendi, Phys. Rev. B **53**, 16 347 (1996).

[6] M. Nirmal, D. J. Norris, M. Kuno, M. G. Bawendi, Al. L. Efros, and M. Rosen, Phys. Rev. Lett. **75**, 3728 (1995); M. Nirmal, C. B. Murray, and M. G. Bawendi, Phys. Rev. B **50**, 2293 (1994); M. G. Bawendi, P. J. Carroll, W. L. Wilson, and L. E. Brus, J. Chem. Phys. 96, 946 (1992).

[7] A. I. Ekimov, F. Hache, M. C. Schanne-Klein, D. Ricard, C. Flytzanis, I. A. Kudryavtsev, T. V. Yazeva, A. V. Rodina, and Al. L. Efros, J. Opt. Soc. Am. B **10**, 100 (1993).

[8] L. Brus, Appl. Phys. A **53**, 465 (1991).

[9] T. Takagahara, Optoelect. Dev. Tech. **8**, 545 (1993); T. Takagahara, Surf. Sci. **267**, 310 (1992); Y. Kayanuma, J. Phys. Soc. Jpn. **62**, 346 (1993).

[10] D. Heitmann and J. P. Kotthaus, Phys. Today **46**(6), 56 (1993).

[11] S. Lloyd, Science **261**, 1569 (1993).

[12] Y. Arakawa and T. Takahashi, Optoelectronics **3**, 155 (1988); Y. Arakawa, in *Confined Electrons and Photons*, Vol. 340 of *NATO Advanced Study Institute, Series B: Physics*, edited by E. Burstein and C. Weisbuch (Plenum, New York, 1995), p. 647; R. Ugajin, J. Appl. Phys. **76**, 2833 (1994).

[13] V. Colvin, M. Schlamp, and A. P. Alivisatos, Nature **370**, 354 (1994); B. O. Dabbousi, M. G. Bawendi, O. Onitsuka, and M. F. Rubner, Appl. Phys. Lett. **66**, 11 (1995).

[14] B. O'Regan and M. Grätzel, Nature **353**, 737 (1991); G. Redmond, D. Fitzmaurice, and M. Graetzel, Chem. Mater. **6**, 686 (1994); G. Hodes, I. D. J. Howell, and L. M. Peter, J. Electrochem. Soc. **139**, 3136 (1992).

[15] R. Leon, P. M. Petroff, D. Leonard, and S. Farad, Science **267**, 1966 (1995).

[16] C. B. Murray, C. R. Kagan, and M. G. Bawendi, Science **270**, 1335 (1995); T. Vossmeyer, G. Reck, L. Katsikas, E. T. K. Haupt, B. Schulz, and H. Weller, *ibid*. **267**, 1476 (1995).

[17] C. B. Murray, C. R. Kagan, and M. G. Bawendi (unpublished).

[18] C. R. Kagan, C. B. Murray, M. Nirmal, and M. G. Bawendi, Phys. Rev. Lett. **76**, 1517 (1996).

[19] J. E. Bowen Katari, V. L. Colvin, and A. P. Alivisatos, J. Phys. Chem. **98**, 4109 (1994); L. R. Becerra, C. B. Murray, R. G. Griffin, and M. G. Bawendi, J. Chem. Phys. **100**, 3297 (1994).

[20] A. Guinier, *X-Ray Diffraction* (Dover, New York, 1994), p. 319.

[21] H. P. Klug and L. E. Alexander, *X-Ray Diffraction Procedures* (Wiley, New York, 1954), p. 586.

[22] V. M. Agranovich and M. D. Galanin, *Electronic Excitation Energy Transfer in Condensed Matter* (North-Holland, New York, 1982); Th. Förster, in *Comparative Effects of Radiation*, edited by M. Burton, J. S. Kirby-Smith, and J. L. Magee (Wiley, New York, 1960), p. 301; D. L. Dexter, J. Chem. Phys. **21**, 836 (1953).

[23] M. W. Windsor, *Physics and Chemistry of the Organic Solid State* (Interscience, New York, 1965), Vol. 2, p. 343.

[24] A. A. Lamola, *Energy Transfer and Organic Photochemistry* (Interscience, New York, 1969), Vol. 14, p. 17.

[25] Refractive indices for the CdSe cores are calculated from the Moss rule $n^4 = 77/E_g$ (eV) using the temperature-dependent bulk E_g (Ref. 26).

[26] *Numerical Data and Functional Relationships in Science and Technology*, edited by K. H. Hellwege, Landolt-Börnstein, New Series, Group III, Vol. 17, Pt. b (Springer-Verlag, Berlin, 1982).

[27] *Dictionary of Organophosphorous Compounds*, edited by R. S. Edmundson (Chapman and Hall, New York, 1988), p. 828.

[28] We assume that at RT the distribution of decay rates originates from a distribution in nonradiative lifetimes.

[29] R. C. Powell, J. Lumin. **11**, 1 (1975); S. I. Golubov and Yu. V. Konobeev, Phys. Status Solidi B **79**, 79 (1977).

[30] G. Liu and J. E. Guillet, Macromolecules **23**, 1388 (1990).

[31] C. R. Kagan, C. B. Murray, and M. G. Bawendi, in *Microcrystalline and Nanocrystalline Semiconductors*, edited by L. Brus, M. Hirose, R. W. Collins, F. Koch, and C. C. Tsai, MRS Symposia Proceeding No. 358 (Materials Research Society, Pittsburgh, 1995), 219; L. Spanhel and M. A. Anderson, J. Am. Chem. Soc. **112**, 2278 (1990).

[32] T. Pullerits and A. Freiberg, Chem. Phys. **149**, 409 (1991); Biophys. J. **63**, 879 (1992); O. J. G. Somsen, F. van Mourik, R. van Grondelle, and L. Valkunas, *ibid*. **66**, 1580 (1994).